
# Electrostatic polyelectrolyte-myoglobin complexes: relaxation dynamics and viscosity under hydrated and aqueous conditions

Soft Matter

ROYAL SOCIETY OF CHEMISTRY

PAPER

Published on 13 July 2026




Cite this: *Soft Matter*, 2026, **22**, 5338

# Electrostatic polyelectrolyte–myoglobin complexes: relaxation dynamics and viscosity under hydrated and aqueous conditions

Achilleas Pipertzis,[a]* Angeliki Chroni,[b] Andrzej Marcinkowski,[c] Barbara Trzebicka,[c] Stergios Pispas[b]* and Jan Swenson[a]*

Received 13th May 2026,
Accepted 12th July 2026

DOI: 10.1039/d6sm00449k

rsc.li/soft-matter-journal

This study investigates the structural characteristics of polyelectrolyte–protein electrostatic complexes and their impact on molecular relaxation dynamics and viscosity. A synthetic polyelectrolyte, based on a statistical copolymer comprising positively charged poly(vinyl benzyl trimethylammonium chloride) (PVBTMAC) and poly[oligo(ethylene glycol) methacrylate] (POEGMA), was combined with the globular protein myoglobin. By employing atomic force microscopy (AFM) and X-ray scattering techniques, we report the formation of nanoscale electrostatic core–shell assemblies with characteristic sizes of approximately 50 nm and an average interparticle distance of about 60 nm, along with the presence of larger aggregates in the range of 200–250 nm. This complex formation causes the glass transition related dynamics of the copolymer to slow down, due to strong electrostatic interactions between the charged copolymer segments and the globular protein molecules. These strong ionic interactions distinctly increase the glass transition temperature ($T_g$) of the copolymer by about 15 K. By rheological and ball viscometry measurements, we observe an increase in macroscopic viscosity, consistent with the formation of electrostatic complexes and their subsequent aggregation. Overall, these findings provide insight into the interactions between a charged synthetic copolymer and a globular protein, contributing to a deeper understanding of the structure–dynamics–property relationships governing polyelectrolyte–protein electrostatic complexes.

## 1. Introduction

Protein–polyelectrolyte (PE) complexation represents a versatile class of soft-matter systems.[1–12] The phase behavior and structure of protein–PE complexes depend sensitively on the charge density, macromolecular architecture and hydrophobicity of the polyelectrolyte, as well as the heterogeneous surface charge distribution of the protein, among other factors.[1–6] In general, proteins are polyampholytes or inherently zwitterionic macromolecules, possessing special intramolecular and supramolecular structuration with patches of both negative and positive charges on their surfaces, which significantly influence the interaction with charged synthetic/natural polymers. As it is well-evidenced, the structure and the characteristics of the protein–PE complexes are mainly governed by electrostatic interactions.[7–10,13]

While electrostatic attraction is the primary driving force of complex formation, non-electrostatic contributions such as hydrophobic interactions and hydrogen bonding can significantly influence both complex morphology and protein stability.[1,5,14–16] Depending on the balance of these interactions, complexation may lead to soluble aggregates or induce phase separation *via* coacervation (*e.g.* liquid–liquid) or precipitation (*e.g.* solid–liquid). Of particular interest is complexation occurring on the "wrong side" of the protein isoelectric point, where both species carry the same net charge, underscoring the importance of protein surface charge heterogeneity.[17]

Complexation between double hydrophilic block copolymers (DHBCs) and proteins can yield sophisticated nanostructures.[18] DHBCs, composed of two water-soluble host constituents of different chemical natures, are of significant importance in the fields of (bio)materials science, pharmacy, biochemistry, and polymer science.[19–23] They serve as an alternative to classical amphiphilic block copolymers. DHBCs with a charged block(s), or neutral-ionic block polyelectrolytes, exhibit unique and fascinating properties, rendering them good candidates as

[a] *Department of Physics and Astronomy, Chalmers University of Technology, 41296, Gothenburg, Sweden. E-mail: achilleas.pipertzis@chalmers.se, jan.swenson@chalmers.se*

[b] *Theoretical and Physical Chemistry Institute, National Hellenic Research Foundation, 48 Vassileos Constantinou Ave., 11635 Athens, Greece. E-mail: pipspas@eie.gr*

[c] *Centre of Polymer and Carbon Materials, Polish Academy of Sciences, M. Curie-Skłodowskiej Str., 34, 41-819 Zabrze, Poland*

delivery nano-systems of biomacromolecules through electrostatic complexation.[23,24] As it was recently evidenced, cationic DHBCs, synthesized using a reversible addition–fragmentation chain transfer (RAFT) polymerization process, are able to interact electrostatically with charged proteins (*i.e.* insulin).[21] It has been demonstrated that the electrostatic interactions between the charged block and the oppositely charged entities dictate the self-assembly and characteristics of the complexes.[21,22]

Additionally, most DHBCs designed for biomedical applications typically feature a bioeliminable nonionic block, such as poly(ethylene glycol) or poly(oligo ethylene glycol methacrylate) (POEGMA), to promote water solubility and improved stabilization in aqueous media.[21–23,25] POEGMA is a family of biocompatible homopolymers and their monomers are not toxic, making them safer for use in biomedicine.[26] In general, the introduction of a second neutral soluble block influences the solution behaviour of the block polyelectrolyte and hence the complexation process, and at the same time provides the opportunity of better controlling the structure and solution properties of the formed complexes.

From a soft-matter perspective, protein–polyelectrolyte complexes provide a model platform for studying interactions between charged heterogeneous macromolecules in aqueous environments.[21–23,25] In particular, block polyelectrolytes with neutral–ionic architectures enable additional control over complexation behavior and often give rise to core–shell assemblies, in which a complexed water-insoluble core is stabilized by a corona of neutral chains. Such systems display diverse structural characteristics and tunable solution properties. Protein-containing polyelectrolyte complexes have been applied to a wide range of fields: food science, drug delivery, protein purification and enzymatic nanoreactors.[21,25,27–30] Beyond their biological and technological significance, these systems offer fundamental insight into electrostatic self-assembly and structure formation in soft condensed matter.

The case of statistical double hydrophilic copolymers has not received considerable attention so far despite the fact that a statistical arrangement of charged and neutral segments along with the synthetic copolymer chain may influence the mode of interactions and structure formation with proteins. It can be said that random/statistical copolymers mimic more closely the arrangement of amino acid residues in protein molecules compared to diblock copolymers, where charged and neutral segments are present in block sequences. However, despite their relevance for biomacromolecular interactions, the influence of hydration on the structure, molecular dynamics, and viscoelastic properties of protein complexes formed with statistical double hydrophilic copolymers remains poorly understood. In particular, the relationship between nanoscale organization, dielectric relaxation dynamics, and macroscopic rheological response in such systems has not been systematically investigated.

The present work aims to address this gap by studying aqueous solutions of a random double hydrophilic copolymer based on charged/ionic VBTMAC segments and neutral OEGMA segments using differential scanning calorimetry (DSC), atomic force microscopy (AFM), small-angle X-ray scattering (SAXS), dielectric spectroscopy (DS) and rheological measurements. The aim of this study is to elucidate the impact of adding a protein (*i.e.* myoglobin) on their physical properties, ranging from microscopic relaxation dynamics to meso-scale organization and to macroscopic solution's viscosity. We report the formation of electrostatic complexes as well as the presence of larger aggregates, formed through primarily electrostatic interactions between the synthetic charged copolymer and the globular protein, as structurally shown by AFM measurements. This complex formation distinctly slows down the copolymer's relaxation dynamics and increases the viscosity of the solutions and hydrated gels. The obtained results establish correlations between nanoscale morphology, relaxation dynamics, and macroscopic viscoelastic behaviour, thereby providing insight into the structure–dynamics–property relationships governing hydrated polymer–protein assemblies. Such understanding is important for the design of responsive polymer–protein complexes and biomaterials with tunable functional properties.

## 2. Experimental methods

### 2.1. Synthesis

The synthetic procedure and molecular characterization of the P(OEGMA$_{80}$-*co*-VBTMAC$_{20}$) copolymer is highlighted in previous studies.[31, 32] Specifically, a charged copolymer with densely grafted macromolecular architecture was prepared by RAFT polymerization, an advantageous method for controlling the molar mass ($M_w$) and achieving dispersity values close to unity. The chemical structure of the investigated statistical copolymer is shown in Fig. 1, along with a schematic representation depicting the procedure followed for preparing the solutions of the copolymer in water and in the presence of myoglobin in aqueous media.

Equine heart myoglobin ($\geq$ 90% purity, essentially salt-free, lyophilized powder; $\leq$ 10% water), purchased from Sigma-Aldrich (PC code: 1003414746, source: SLCH8120), was used without further treatment. A copolymer-to-myoglobin weight ratio of 2 : 1 was prepared in solutions with varying water concentrations (10 wt%, 30 wt%, 70 wt%, and 90 wt%), depending on the requirements of each experimental technique. The exact concentrations used in each experimental method are provided in Table S1. The isoelectric point of the used protein is around 6.8–7.2, indicating a neutral net charge, but with the presence of patches with different charges on the protein

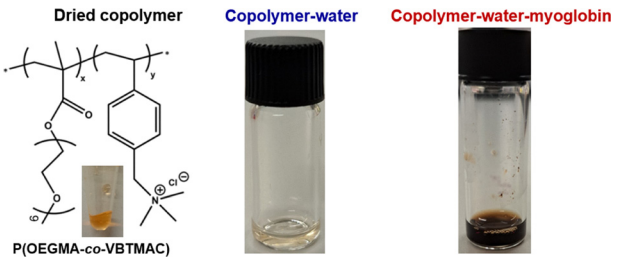


Fig. 1 Chemical structure of the statistical copolymer and digital images of the dried copolymer, copolymer-water solution and copolymer-water-myoglobin solution.

surface. Since the pH of the prepared solutions and hydrated samples was not directly controlled and it was approximately 7 ± 1, myoglobin is expected to remain close to its isoelectric state throughout the experiments.

### 2.2. Dielectric spectroscopy (DS)

DS measurements were carried out using a Novocontrol Alpha frequency analyzer. The temperature protocol involved measurements from 173 K to 423 K in steps of 5 K and for frequencies ranging from $10^{-2}$ to $10^{7}$ Hz, under atmospheric pressure. The measurements were performed using a liquid parallel plate sample cell (with code BDS 1308), provided by Novocontrol. Specifically, the sample dielectric cell comprised two electrodes, each 20 mm in diameter, with the sample held at a thickness of 100 μm by Teflon spacers. The complex dielectric permittivity $\varepsilon^* = \varepsilon' - i\varepsilon''$, where $\varepsilon'$ is the real and $\varepsilon''$ is the imaginary part, was obtained as a function of frequency, $\omega$, temperature, $T$, and pressure, *P i.e.*, $\varepsilon^*(T, \omega)$.[33] The measured relaxation dynamics were fitted by the empirical equation of Havriliak and Negami (HN):[34]

$$\varepsilon^*_{\mathrm{HN}}(\omega, T) = \varepsilon_\infty(T) + \sum_{j=1}^{3} \frac{\Delta\varepsilon(T)}{\left[1 + \left(i\omega \cdot \tau_{\mathrm{HN}_j}(T)\right)^{m_j}\right]^{n_j}} + \frac{\sigma_0(T)}{i\varepsilon_{\mathrm{f}}\omega} \tag{1}$$

where $\varepsilon_\infty(T)$ is the high-frequency permittivity, $\tau_{\mathrm{HN}}(T)$ is the characteristic relaxation time in this equation, $\Delta\varepsilon(T) = \varepsilon_0(T) - \varepsilon_\infty(T)$ is the relaxation strength, $m$ and $mn$ (with limits $0.2 < m$, $mn \leq 1$) describe the symmetrical and asymmetrical broadening, respectively, of the distribution of relaxation times, $\sigma_0$ is the dc conductivity, and $\varepsilon_{\mathrm{f}}$ is the permittivity of free space. From $\tau_{\mathrm{HN}}$, the relaxation time at maximum loss, $\tau_{\max}$, is obtained analytically as follows:[35]

$$\tau_{\max} = \tau_{\mathrm{HN}} \sin^{-1/m}\left(\frac{\pi m}{2(1+n)}\right) \sin^{1/m}\left(\frac{\pi mn}{2(1+n)}\right) \tag{2}$$

For the analysis of the dynamic behaviour, we used the imaginary part of the electric modulus, $M''$. The latter representation facilitates tracking the proton-transport into the bound water that is coupled to the copolymer–protein dynamics. In ion/proton conducting systems, the imaginary part of the complex electric modulus, $M''$, emphasizes contributions from ion/proton motions (ranging from long- to short-/localized-distances), which are associated with the conductivity process. From the maximum of $M''$, the characteristic relaxation time of proton transport can be extracted, by employing the empirical function suggested by Kohlrausch and Williams and Watts given by:

$$\Phi(t) = \exp\left[-\left(\frac{t}{\tau_\sigma}\right)^{\beta_{\mathrm{KWW}}}\right] \tag{3}$$

where, $t$, is the time, $\tau_\sigma$ is the characteristic conductivity relaxation time and $\beta_{\mathrm{KWW}}$ ($0 < \beta_{\mathrm{KWW}} < 1$) is the shape parameter related to the broadening of the relaxation peak. Lower values of $\beta_{\mathrm{KWW}}$ denote a more stretched relaxation process, which corresponds to a broader and more asymmetric peak in the frequency domain. As proposed earlier by Bergman, the $M''$ peak can be directly fitted in the frequency domain, with the following function:[34]

$$M'' = \sum_n \frac{M''_{\max,n}}{(1-\beta_n) + (\beta_n/(1+\beta_n))\left[\beta_n\left(\omega_{\max,n}/\omega\right) + \left(\omega/\omega_{\max,n}\right)^{\beta_n}\right]} \tag{4}$$

where $M''_{\max}$ is the peak value of $M''$ and $\omega_{\max}$ is the corresponding frequency at the maximum of the electric modulus spectra, which is related to the corresponding dielectric relaxation time as $\tau_\sigma = 1/\omega_{\max}$. Representative spectra are shown in Fig. S1(a). Moreover, we employed the real part of the complex conductivity, $\sigma'$, to determine the values of the proton/ionic-conductivity, as depicted in Fig. S1(b).

### 2.3. Viscometry

For the viscosity measurements of the solutions with high water concentrations ($c_{\mathrm{w}} > 80$ wt%), a Lovis M2000 microviscometer from Anton Paar was used. A short-distance sample capillary with a diameter of 1.59 mm and a stainless-steel ball with a diameter of 1.5 mm were employed. The capillary was carefully filled with a syringe, to avoid the formation of air bubbles. At each temperature, an automatic scan of different angles (ranging from −70° to 70°) was performed. All measurements were conducted at atmospheric pressure.

### 2.4. Atomic force microscopy (AFM)

AFM measurements were performed using a Dimension ICON AFM microscope equipped with a NanoScope V controller (BRUKER Corporation, Santa Barbara, CA, US) operating in the soft tapping mode in an air atmosphere with a standard 125 μm long, with flexural stiffness of 42 N m$^{-1}$ of a single-crystal doped silicon cantilevers (Model PPP-NCH-10, NANOSENSORS). Images were obtained using a piezoelectric scanner with a nominal size of 85 × 85 μm. The micrographs were recorded using NanoScope Analysis 1.9 Software (BRUKER Corporation, Santa Barbara, CA, US).

For AFM measurements, sample solutions were dripped onto the surface of freshly split mica and left to dry at room temperature. For the samples, 2D and 3D images were acquired from surface areas of 0.5 × 0.5 μm and 4.0 × 4.0 μm. A z-scale ranging from −10 to +10 nm was maintained for all images.

### 2.5. Small-angle X-ray scattering

SAXS measurements were conducted using a Mat:Nordic instrument (SAXSLAB) at Chalmers Material Analysis Laboratory (CMAL), for identifying the self-assembly of the solution with myoglobin. The measurements were carried out under vacuum at room temperature. The solution was placed in a 1.5 mm quartz capillary tube using a syringe. The exposure time was 30 min and a sample–detector distance of ∼1.08 m was used, which gives a $q$-range of 0.0138–3.0717 nm$^{-1}$.

# 3. Results and discussion

## 3.1. Structural evidence of polyelectrolyte–myoglobin complexes

For structurally identifying the formation and characteristics of the copolymer–protein electrostatic complexes, AFM and SAXS measurements were performed, as detailed in the "Experimental methods" section (Fig. 2). Due to its high sensitivity, AFM enables the detection of individual binding events as well as the investigation of intermolecular and intramolecular interactions.[36,37] To identify these polyelectrolyte–myoglobin complexes, AFM measurements were conducted using dried solutions, and representative images are shown in Fig. 2. Results for the dried solution without myoglobin indicate the absence of aggregates, reflecting the hydrophilic nature of the copolymer (Fig. S2).

For the copolymer-water solution, a very smooth surface can be observed without visible objects or changes in texture, regardless of the location (layer thickness) and size of the scanned area, as depicted in Fig. S2. For the specimen containing myoglobin, a heterogeneous surface texture was observed with differences in height between 3 nm and 7 nm and objects in two ranges of diameter 50–60 nm, indicating the formation of primarily core–shell assemblies, and 200–250 nm, reflecting further aggregation of the smaller complexes, as shown in Fig. 2a and detailed below. Using the AFM technique, the complex of myoglobin and polystyrene nanoparticles[38] and the adsorption of myoglobin onto phosphate-grafted zirconia nanoparticles were studied.[39]

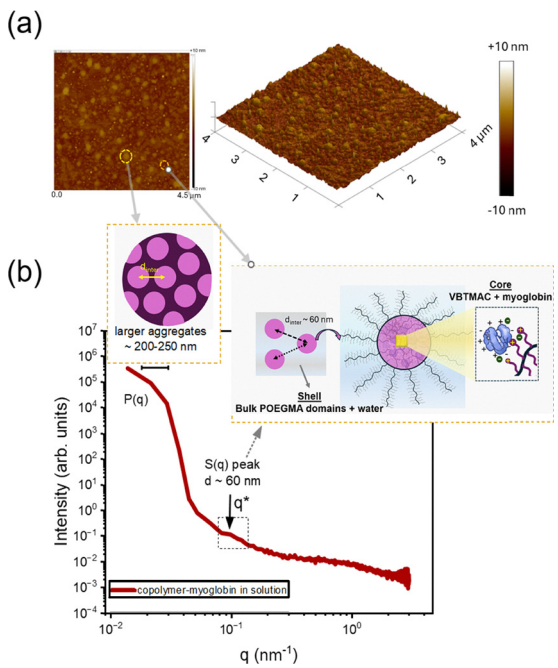


Fig. 2 (a) 1D and 2D AFM images and (b) SAXS pattern of the solution with myoglobin. The specific concentrations used for each experiment are provided in Table S1. In (b), the different size populations and characteristic distances observed in AFM and SAXS are illustrated. The error bars of the SAXS data are given by the line thickness.

Quantitative insight into the structure and the presence of these electrostatic complexes can also be obtained through SAXS measurements. The SAXS patterns of the solution containing myoglobin ($c_w$ = 90 wt%) are provided in Fig. 2b.

In the SAXS data, the scattered intensity is given by the product:[40]

$$I(q) \sim KP(q)S(q) \quad (5)$$

where $P(q)$ is the form factor and $S(q)$ is the structure factor, and $K$ is a constant that depends on the particle concentration, the scattering contrast between the particles and the solvent, and instrumental factors. The structure factor is associated with the peak at around 0.1 $nm^{-1}$ that corresponds to a distance of $d = 2\pi/q^* \approx 60$ nm and reflects the inter-micellar or inter-spheres distance, as depicted in the schematic representation in Fig. 2. Alternatively, this characteristic distance may be attributed to the size of the smaller aggregates observed in the AFM measurements. However, the former interpretation appears more plausible. In particular, the corresponding peak coincides with the nanophase separation distance between the charged domains and the neutral bulk POEGMA regions, as evidenced in our previous study.[32]

The low-$q$ regime corresponds to the Guinier region, which is associated with the overall size of the scattering objects. In this region, the scattering intensity mainly arises from the form factor. This region corresponds to particle diameters of the order of 200–250 nm, which is in good agreement with the larger aggregates observed in the AFM measurements. It needs to be mentioned that the AFM measurements were performed in dried solutions, facilitating the formation of larger complexes. Taken together the X-ray scattering and AFM results suggest a hierarchical organization/self-assembly: primary copolymer–protein complexes with characteristic sizes of about 50–60 nm and a periodic distance between them of 60 nm, which further associate to form larger aggregates with sizes in the range of 200–250 nm. Therefore, the structural data verify the formation of electrostatic complexes as well as the formation of larger aggregates. An open question that immediately arises is how the presence of these smaller and larger aggregates affects the molecular dynamics and the intrinsic viscosity of our systems.

## 3.2. Protein–copolymer relaxation dynamics

Isothermal dielectric measurements were carried out to gain insight into the impact of copolymer–protein aggregates on the $T_g$-related dynamics. Dielectric spectroscopy primarily reflects reorientational motions of molecular dipoles and translational motions of charge carriers. However, the presence of solvent, which enhances the conductivity through charge transport and imparts first order transitions, can further complicate the distinction between different types of motions. Strategies to mitigate these undesirable solvent effects include confining the solvent within nanoscale cavities to promote a fully amorphous state or reducing the solvation level in hydrated systems to limit solvent-related contributions and first-order transitions, as detailed below, by varying the solvation level in our systems.

At the same time, the presence of water (*i.e.* solvent) is essential for structure, dynamics, and functions of proteins, in contrast to synthetic polyelectrolytes, which can be studied under dried conditions.[31,32,41–44] The hydration level has a strong effect on the relaxation dynamics of proteins and on their specific biological role.[45] It has been demonstrated that their specific function is lost in the dehydrated state, and a solvent concentration higher than 20 wt% is required for detectable biological activity.[41–44] The reason for this is that without water (or another suitable solvent) a protein shows no biologically important dynamics, and as a result, it cannot perform any biological activities.[43,46] The water molecules surrounding a protein strongly interact with the protein surface by forming hydrogen bonds to the main chain or the side chain functional groups of the protein. Additionally, the motions of water molecules govern the flexibility of the protein, which is necessary for their function.[41,45] Therefore, it is necessary to select an optimal water content that both preserves the protein's functionality and allows monitoring the $T_g$-related dynamics of the copolymer.

**3.2.1. Effect of water concentration on the $T_g$-related dynamics.** The extracted relaxation times of the electric modulus representations and the values of proton/ionic conductivities are plotted as a function of inverse temperature in Fig. 3 and Fig. 4, for the solutions with different water concentrations.

As depicted in Fig. 3 and 4, the $\sigma$-/$\alpha$-process coincides with copolymer's segmental process at very low water contents.[32] For $c_w < 40$ wt%, the temperature dependence of relaxation times and dc-conductivities follow the Vogel–Fulcher–Tammann equation according to:

$$\tau_{max} = \tau_0^{\#} \exp\left(\frac{B}{T - T_0}\right) \quad (6)$$

$$\sigma_{max} = \sigma_0^{\#} \exp\left(-\frac{B}{T - T_0}\right) \quad (7)$$

where $\tau_0^{\#}\left(\sigma_0^{\#}\right)$ is the relaxation time (conductivity) in the limit of an infinitely high temperature, $B$ is the activation parameter, and $T_0$ is the ideal glass transition temperature located below the conventional $T_g$, dielectrically defined as the temperature where the relaxation time reaches 100 s. The VFT parameters of the relaxation maps (*i.e.* temperature dependence of relaxation times) along with the dielectric $T_g$s are summarized in Table S2.

The VFT temperature dependence, indicative of cooperative structural dynamics associated with the glass transition temperature, combined with the convergence of relaxation dynamics with the segmental copolymer's dynamics at very low hydration levels, suggests a coupling between ion/proton transport and the structural dynamics of the copolymer (copolymer–myoglobin). Under low hydration conditions, water is predominantly quasi-bound to the copolymer chains. This fraction remains non-freezable, and proton transport is therefore facilitated through this hydration water, which is dynamically coupled to the polymer matrix, as illustrated in Fig. 3. With increasing water content, the $T_g$-related dynamics speed up and thus $T_g$ decreases, reflecting the plasticization effect of the water solvent, as shown in Fig. S3a.

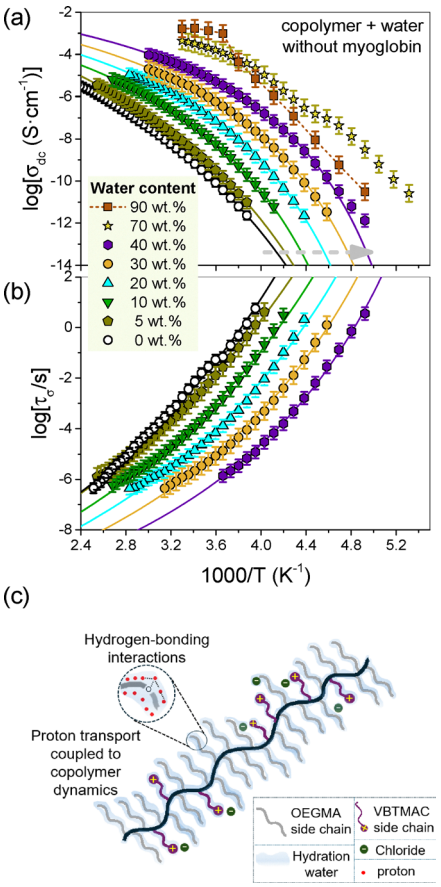


Fig. 3 Inverse temperature dependence of (a) dc-conductivity and (b) relaxation times for the copolymer solutions without myoglobin, bearing diferent water concentrations; 90 wt% (brown squares), 70 wt% (yellow stars), 40 wt% (purrple hexagons), 30 wt% (orange circles), 20 wt% (cyan up-trangles), 10 wt% (green down-triangles), 5 wt% (dark-yellow pentagons) and 0 wt% (black circles). The solid lines represent fits by eqn (7) and (6), respectively. (c) Schematic representation of the copolymer structure and its hydration water, where the proton transport is coupled to the copolymer relaxation dynamics, which is facilitated by water.

In contrast, at water contents exceeding 40 wt%, the presence of freezable and bulk-like water domains (see Fig. 3 and 4) leads to discontinuities in the temperature dependence of both the dc conductivity and the relaxation times associated with the $\sigma$-/$\alpha$-process. Notably, at these higher hydration levels, a decoupling between proton transport and structural dynamics is observed. Concurrently, the proton conductivity increases (Fig. S3b), reflecting the increased number density of protons and the formation of water clusters, facilitating the transport of protons. In this case, the proton transport is facilitated by the hydrogen-bond-forming networks of water. The proton migration is mainly facilitated through the proton hopping (protons are passed along the hydrogen bonds) according to the Grotthuss mechanism.[47] Therefore, an intermediate water content between the limits of 20 wt% (*i.e.* loss of protein functionality) and 40 wt% (decoupling of proton

 

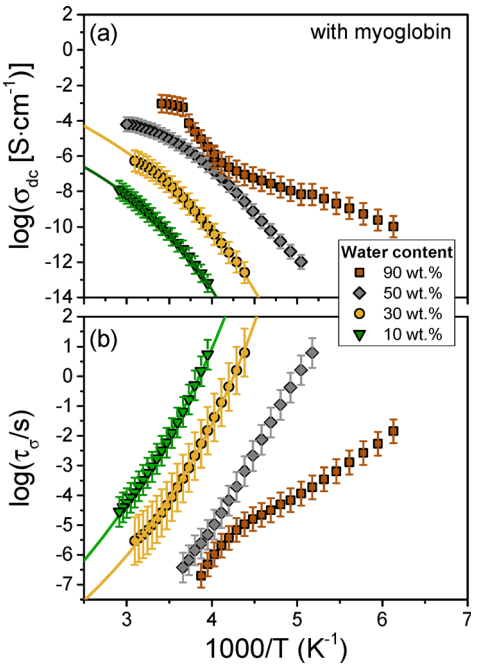


Fig. 4 Inverse temperature dependence of (a) dc-conductivity and (b) relaxation times for the copolymer-myoglobin solutions with different water concentrations; 90 wt% (brown squares), 50 wt% (grey squares), 30 wt% (orange circles) and 10 wt% (green down-triangles), upon heating. The solid lines represent fits by eqn (7) and (6), respectively.

transport from copolymer dynamics) is required for gaining insight into the effect of polymer–protein electrostatic interactions on the $T_g$-related dynamics.

**3.2.2. Impact of copolymer–protein interactions and aggregates on the $T_g$-related dynamics.** Fig. 5 illustrates 3D-representations as a function of frequency and temperature of the copolymer solutions with and without protein, at a fixed water concentration of 30 wt%.

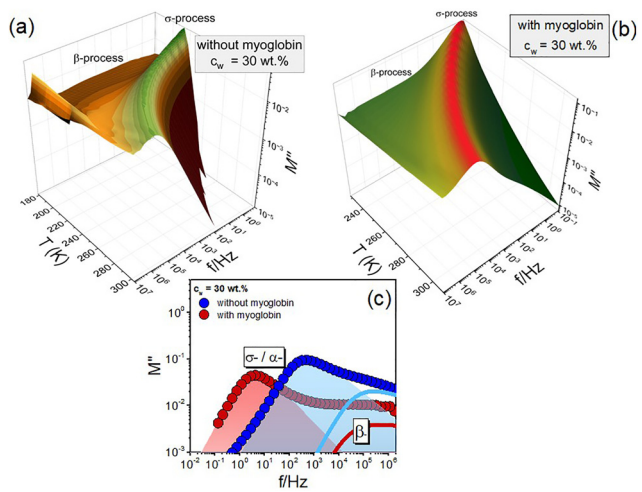


Fig. 5 (a) and (b) 3D-representation of the electric modulus spectra as a function of frequency and temperature for solutions of copolymer-water without (a) and with (b) myoglobin, at a water concentration of 30 wt% and in the temperature ranges of 178–303 K and 228–323 K for the solutions without and with myoglobin, respectively. (c) Comparison of electric modulus spectra at $T$ = 253 K. The coloured areas and solid lines represent fits by eqn (4), for the $\sigma$-/$\alpha$- and $\beta$-process, respectively.

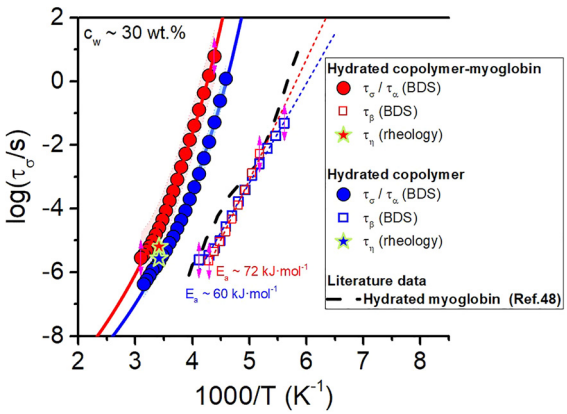


Fig. 6 Relaxation times as a function of inverse temperature for hydrated ($c_w$ = 30 wt%) myoglobin (dashed line), copolymer (blue symbols) and copolymer–myoglobin (red symbols). The dielectric data of myoglobin-water were taken from the literature, ref. 48. Relaxation times calculated from rheological viscosity data (yellow stars) are also provided for comparison.

The relaxation times at the maximum of electric modulus spectra, extracted using eqn (4), are plotted as a function of inverse temperature in Fig. 6. The relaxation times of the myoglobin–water hydrated system, taken from the literature, are also provided for comparison.[48]

The temperature dependence of relaxation times for the $\sigma$-/$\alpha$-process follows eqn (6), and the VFT parameters along with the values of the extracted dielectric $T_g$s are provided in Table 1. As shown in Fig. 6, the interactions between the copolymer and the protein molecules result in slowing down of the copolymer's $T_g$-related relaxation dynamics. Specifically, at a fixed temperature, the relaxation time decreases by about 1 order of magnitude, reflecting the formation of protein–copolymer complexes as well as the presence of larger aggregates, as structurally shown in Fig. 2. It indicates a dominance of strong electrostatic/ionic interactions between the charged PVBTMAC block and myoglobin, over the steric hindrance or hydrophobic interactions. These strong ionic interactions distinctly increase the value of $T_g$ by about 15 K. However, it should be noted here that also redistributions of counterions and water molecules may contribute to this slowing down of the copolymer's segmental dynamics since it has, for instance, been shown that myoglobin has a strong tendency to be preferentially hydrated.[49] Thus, it is possible that the water prefers to interact

Table 1 VFT parameters, dielectric glass transition temperature and fragility for the hydrated systems with and without myoglobin, at $c_w$ = 30 wt%

| Code | $-\log(\tau_0/s)^a$ | $B$ (K) | $T_0$ (K) | $T_g$ (K) ($\tau$ = 100 s) | $m$* |
|---|---|---|---|---|---|
| Without myoglobin | 12 | 2310 ± 30 | 134 ± 2 | 206 ± 2 | 39.9 |
| With myoglobin | 12 | 2690 ± 20 | 137 ± 1 | 221 ± 1 | 36.6 |

[a] Held fixed.

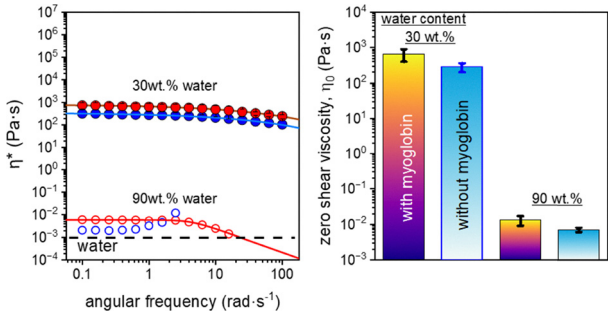


Fig. 7 (a) Dynamic frequency sweeps for the solutions without (blue) and with myoglobin (red) at two water concentrations: 30 wt% (filled symbols) and 90 wt% (open symbols). The solid lines represent fits by eqn (8). (b) Extracted values of zero-shear viscosity for the solutions without myoglobin (cyan bars) and with myoglobin (multicolored bars). At $c_w \sim$ 90 wt%, the zero-shear viscosity was verified by performing ball microviscometry measurements.

with myoglobin rather than the copolymer, thereby reducing the effective hydration level of the copolymer, which, in turn, slows down its segmental dynamics.

To quantify the temperature dependence of this structural process at $T_g$, the fragility (or steepness index) can be calculated as $m^* = BT_g/[2.303(T_g - T_0)^2]$.[50,51] The values are provided in Table 1. The formation of copolymer–protein electrostatic complexes reduces the fragility, reflecting their stronger nature.

Furthermore, a faster relaxation mode exhibiting an Arrhenius temperature dependence can be observed, which is characteristic of local, non-cooperative motions occurring in the glassy state. The corresponding activation energy is approximately 60–70 kJ·mol$^{-1}$. A similar relaxation process has previously been observed for hydrated lysozyme[52] and myoglobin[48,53] and it has been ascribed to relaxation of polar side groups in the protein. In our case, we cannot exclude contributions from the polar moieties located at the copolymer's side chains to this relaxation. Here, it should be noted that there is also a faster, partly overlapping, relaxation process due to the dynamics of the hydration water. However, this water relaxation has been omitted in Fig. 6 since it is difficult to determine its exact temperature dependence, due to the mentioned overlap with the $\beta$-relaxation.

Overall, the strong electrostatic interactions between the globular protein molecules and the charged segments of the random copolymer significantly influence the microscopic molecular dynamics. However, several questions remain unresolved, particularly regarding the precise nature of the $T_g$-related process and its relationship to the intrinsic viscosity of the solution. Furthermore, the extent to which copolymer–protein aggregation affects the macroscopic viscosity of the solution requires further investigation.

### 3.3. Mechanical properties of hydrated copolymers

To address the aforementioned points, rheological measurements and ball viscometry were conducted. The formation of copolymer–protein electrostatic complexes is anticipated to increase the viscosity of hydrated specimens (*i.e.* $c_w \sim$ 30 wt%) and aqueous solutions (*i.e.* $c_w \sim$ 90 wt%). The zero-shear viscosity, $\eta_0$, was extracted from the frequency-independent regime of complex viscosity, at low frequencies, by performing dynamic frequency sweeps into the linear viscoelastic response (Fig. 7a). Specifically, the viscosity data were fitted with the empirical model of Carreau–Yasuda to estimate the value of zero-shear viscosity, $\eta_0$, according to:[54,55]

$$\eta^*(\omega) = \eta_0[1 + (\lambda\omega)^m]^{\frac{n-1}{m}} \quad (8)$$

where $\lambda$ is the relaxation time, $m$ indicates the width of the transition region between Newtonian and power-law behaviour and $n$ is the power-law index (*i.e.* a measure of the shear-thinning nature of a polymer melt). All these parameters can be obtained by fitting the measured data.

As illustrated in Fig. 7b, the incorporation of myoglobin increases the zero-shear viscosity from 280 ± 80 to 650 ± 200 at 30 wt% water and from 0.007 ± 0.001 to 0.013 ± 0.004 at 90 wt% water. The viscosity data can also provide additional information for the interpretation of the dielectric data. A comparison of the dielectric and rheological data is provided in Fig. 6. The rheological relaxation times were calculated from Maxwell equation, $\tau = \eta/G_\infty$, where $G_\infty$ (= $10^8$ Pa) is the ideal glassy modulus. The convergence of relaxation times of the $\sigma$-/$\alpha$-process with the viscosity data verifies its structural origin, arising from the copolymer's segmental relaxation. In addition, the results from the mechanical measurements support the slowing down of $T_g$-related dynamics, following the incorporation of the protein. This slowing down can be explained by ionic interactions between the globular protein and the charged VBTMAC segments. As it is widely reported in the literature,[56–58] the heterogeneous surface charge distribution of proteins can promote protein–polyelectrolyte complexation and coacervation even when the protein is close to its isoelectric point and possesses an approximately zero net charge. Notably, these strong interactions through the formation of small and large aggregates (see Fig. 2) also distinctly affect the macroscopic viscosity.

To sum up, the dominance of strong ionic interactions between the charged VBTMAC segments randomly arranged along the copolymer backbone and the localized negatively charged patches on the protein surface results in the formation of copolymer–protein electrostatic complexes and larger aggregates, affecting the $T_g$-related molecular dynamics of the copolymer as well as the macroscopic viscosity.

## 4. Conclusions

In this study, we used dielectric spectroscopy, rheology and viscometry, AFM, and SAXS to investigate the influence of strong electrostatic interactions between a positively charged statistical double hydrophilic copolymer and the globular protein myoglobin. The structural characterization studies reveal the formation of copolymer–protein core–shell micellar assemblies with characteristic sizes of approximately 50 nm and an average interparticle distance of about 60 nm. These primary complexes were found to further associate into larger

 

aggregates with sizes in the range of 200–250 nm. To elucidate the effect of these aggregates on the microscopic molecular dynamics, dielectric spectroscopy measurements were conducted. Analysis of the glass transition related dynamics of the copolymer indicates a slowing down of approximately one decade, reflecting the presence of strong electrostatic interactions between the charged VBTMAC segments and the protein molecules. Concurrently, the viscosity of the hydrated systems exhibits a clear correlation with the $T_g$-related dielectric relaxation process, supporting the relation between macroscopic properties and microscopic molecular dynamics. In addition, the viscosity data further highlight the influence of the copolymer–protein aggregation on the macroscopic mechanical properties. These findings demonstrate that electrostatic interactions between the positively charged copolymer and the polyampholytic charge distribution of myoglobin play a dominant role in the complexation/aggregation process. Overall, this work provides insight into the interplay between structure, molecular dynamics, and rheological behaviour in polyelectrolyte copolymer–protein complexes, contributing to a more comprehensive understanding of such systems.

## Author contributions

A. P. contributed to data curation, formal analysis, investigation, methodology, validation, and writing – original draft. A. C. participated in resources and formal analysis. A. M. contributed to data curation, formal analysis, investigation, methodology, and writing – review and editing. B. T. contributed to supervision, data curation, validation, and writing – review and editing. S. P. participated in project administration, supervision, conceptualization, validation, resources, and writing – review and editing. J. S. contributed to project administration, supervision, funding acquisition conceptualization, validation, and writing – review and editing.

## Conflicts of interest

There are no conflicts to declare.

## Data availability

Data will be made available on request.

Supplementary information (SI) is available, containing additional dielectric and AFM data. See DOI: https://doi.org/10.1039/d6sm00449k.

## Acknowledgements

A. P and J. S. thank the Areas of Advance Materials Science and Energy at Chalmers University of Technology for the financial support.

## References

1 J. Y. Gao and P. L. Dubin, Binding of proteins to copolymers of varying hydrophobicity, *Biopolymers*, 1999, **49**, 185–193.
2 J. M. Park, B. B. Muhoberac, P. L. Dubin and J. Xia, Effects of protein charge heterogeneity in protein-polyelectrolyte complexation, *Macromolecules*, 1992, **25**, 290–295.
3 K. W. Mattison, P. L. Dubin and I. J. Brittain, Complex formation between bovine serum albumin and strong polyelectrolytes: effect of polymer charge density, *J. Phys. Chem. B*, 1998, **102**, 3830–3836.
4 D. Takahashi, Y. Kubota, K. Kokai, T. Izumi, M. Hirata and E. Kokufuta, Effects of surface charge distribution of proteins in their complexation with polyelectrolytes in an aqueous salt-free system, *Langmuir*, 2000, **16**, 3133–3140.
5 S. P. Le, J. Krishna, P. Gupta, R. Dutta, S. Li, J. Chen and S. Thayumanavan, *Biomacromolecules*, 2024, **25**, 6229–6249.
6 V. Chrysostomou, A. Forys, B. Trzebicka, C. Demetzos and S. Pispas, Structure of micelleplexes formed between QPDMAEMA-*b*-PLMA amphiphilic cationic copolymer micelles and DNA of different lengths, *Eur. Polym. J.*, 2022, **166**, 111048.
7 M. Berdick and H. Morawetz, The interaction of catalase with synthetic polyelectrolytes, *J. Biol. Chem.*, 1954, **206**, 959–971.
8 H. Morawetz and W. L. Hughes Jr, The interaction of proteins with synthetic polyelectrolytes. I. Complexing of bovine serum albumin, *J. Phys. Chem.*, 1952, **56**, 64–69.
9 H. Morawetz and H. Sage, The effect of poly (acrylic acid) on the tryptic digestion of hemoglobin, *Arch. Biochem. Biophys.*, 1955, **56**, 103–109.
10 A. A. Green and W. L. Hughes, Protein fractionation on the basis of solubility in aqueous solutions of salts and organic solvents, *Methods Enzymol.*, 1955, **1**, 67–90.
11 D. Fotaki, M. Karayianni, A. Skandalis, E. Haladjova, A. Forys, B. Trzebicka, S. Rangelov and S. Pispas, Complexation of poly (methacrylic acid) star polyelectrolytes with lysozyme, *Eur. Polym. J.*, 2024, **206**, 112773.
12 A. D. Presley, J. J. Chang and T. Xu, Directed co-assembly of heme proteins with amphiphilic block copolymers toward functional biomolecular materials, *Soft Matter*, 2011, **7**, 172–179.
13 E. Ganou, M. A. Pantelaiou, V. Chrysostomou, K. Olszowska, B. Trzebicka and S. Pispas, Block Copolymer–Sodium Oleate Complexes Through Electrostatic Interactions for Curcumin Encapsulation, *Materials*, 2025, **18**, 5375.
14 J. Gong, P. Yao, H. Duan, M. Jiang, S. Gu and L. Chunyu, Structural Transformation of Cytochrome *c* and Apo Cytochrome *c* Induced by Sulfonated Polystyrene, *Biomacromolecules*, 2003, **4**, 1293–1300.
15 E. Seyrek, P. L. Dubin, C. Tribet and E. A. Gamble, Ionic strength dependence of protein-polyelectrolyte interactions, *Biomacromolecules*, 2003, **4**, 273–282.
16 Y. Xie, N. Hu and H. Liu, Bioelectrocatalytic reactivity of myoglobin in layer-by-layer films assembled with triblock copolymer Pluronic F127, *J. Electroanal. Chem.*, 2009, **630**, 63–68.

17 S. Gao, A. Holkar and S. Srivastava, Protein–polyelectrolyte complexes and micellar assemblies, *Polymers*, 2019, **11**, 1097.
18 I. K. Voets, A. De Keizer and M. A. C. Stuart, Complex coacervate core micelles, *Adv. Colloid Interface Sci.*, 2009, **147**, 300–318.
19 S. Pispas, Double hydrophilic block copolymers of sodium (2-sulfamate-3-carboxylate) isoprene and ethylene oxide, *J. Polym. Sci. A Polym. Chem.*, 2006, **44**, 606–613.
20 G. Mountrichas and S. Pispas, Novel double hydrophilic block copolymers based on poly(p-hydroxystyrene) derivatives and poly(ethylene oxide), *J. Polym. Sci. A Polym. Chem.*, 2007, **45**, 5790–5799.
21 A. Chroni, A. Forys, T. Sentoukas, B. Trzebicka and S. Pispas, Poly [(vinyl benzyl trimethylammonium chloride)]-based nanoparticulate copolymer structures encapsulating insulin, *Eur. Polym. J.*, 2022, **169**, 111158.
22 A. Chroni, A. Forys, B. Trzebicka, A. Alemayehu, V. Tyrpekl and S. Pispas, Poly[oligo(ethylene glycol) methacrylate]-*b*-poly[(vinyl benzyl trimethylammonium chloride)] Based Multifunctional Hybrid Nanostructures Encapsulating Magnetic Nanoparticles and DNA, *Polymers*, 2020, **12**, 1283.
23 M. Karayianni and S. Pispas, Block copolymer solution self-assembly: Recent advances, emerging trends, and applications, *J. Polym. Sci.*, 2021, **59**, 1874–1898.
24 K. Al-Tahami and J. Singh, Smart polymer based delivery systems for peptides and proteins, *Recent Pat. Drug Deliv. Form.*, 2007, **1**, 65–71.
25 M. Karayianni, R. Radeva, N. Koseva and S. Pispas, Electrostatic complexation of a double hydrophilic block polyelectrolyte and proteins of different molecular shape, *J. Polym. Sci. B Polym. Phys.*, 2016, **54**, 1515–1529.
26 A. Singh, N. Dowdall and T. Hoare, Poly (oligo (ethylene glycol) methacrylate)-based polymers in biomedical applications: Preparation and applications, *Biomacromolecules*, 2025, **26**, 3929–3973.
27 L. G. Santiago and G. R. Castro, Novel technologies for the encapsulation of bioactive food compounds, *Curr. Opin. Food Sci.*, 2016, **7**, 78–85.
28 Z. Li, Y. Wang, Y. Pei, W. Xiong, C. Zhang, W. Xu, S. Liu and B. Li, Curcumin encapsulated in the complex of lysozyme/carboxymethylcellulose and implications for the antioxidant activity of curcumin, *Food Res. Int.*, 2015, **75**, 98–105.
29 N. Eghbal and R. Choudhary, Complex coacervation: Encapsulation and controlled release of active agents in food systems, *LWT - Food Sci. Technol.*, 2018, **90**, 254–264.
30 J. Pathak, K. Rawat, V. Aswal and H. Bohidar, Interactions in globular proteins with polyampholyte: coacervation route for protein separation, *RSC Adv.*, 2015, **5**, 13579–13589.
31 A. Pipertzis, A. Chroni, S. Pispas and J. Swenson, Viscoelastic Response of Double Hydrophilic Block Copolymers for Drug Delivery Applications, *Polymers*, 2025, **17**, 1857.
32 A. Pipertzis, A. Chroni, S. Pispas and J. Swenson, Molecular Dynamics and Self-Assembly in Double Hydrophilic Block and Random Copolymers, *J. Phys. Chem. B*, 2024, **128**, 11267–11276.
33 F. Kremer and A. Schönhals, *Broadband dielectric spectroscopy*, Springer Science & Business Media, 2002.
34 R. Bergman, General susceptibility functions for relaxations in disordered systems, *J. Appl. Phys.*, 2000, **88**, 1356–1365.
35 S. Havriliak and S. Negami, A complex plane representation of dielectric and mechanical relaxation processes in some polymers, *Polymer*, 1967, **8**, 161–210.
36 Q. Wang, L. Liu, X. Yang, K. Wang, N. Chen, C. Zhou, B. Luo and S. Du, Evaluation of medicine effects on the interaction of myoglobin and its aptamer or antibody using atomic force microscopy, *Anal. Chem.*, 2015, **87**, 2242–2248.
37 M. Nattich-Rak, A. Pomorska, P. Batys and Z. Adamczyk, Adsorption kinetic of myoglobin on mica and silica–Role of electrostatic interactions, *Colloids Surf., B*, 2021, **198**, 111436.
38 Z. Adamczyk and M. Nattich-Rak, Formation of Myoglobin Corona at Polymer Microparticles, *Colloids Interfaces*, 2021, **5**, 27.
39 F. Bellezza, A. Cipiciani, M. A. Quotadamo, S. Cinelli, G. Onori and S. Tacchi, Structure, stability, and activity of myoglobin adsorbed onto phosphate-grafted zirconia nanoparticles, *Langmuir*, 2007, **23**, 13007–13012.
40 T. Li, A. J. Senesi and B. Lee, Small angle X-ray scattering for nanoparticle research, *Chem. Rev.*, 2016, **116**, 11128–11180.
41 R. Pethig, Protein-water interactions determined by dielectric methods, *Annu. Rev. Phys. Chem.*, 1992, **43**, 177–205.
42 J. A. Rupley and G. Careri, Protein-water interactions determined by dielectric methods, *Adv. Protein Chem. Struct. Biol.*, 1991, **41**, 37–172.
43 H. Jansson, R. Bergman and J. Swenson, Relation between solvent and protein dynamics as studied by dielectric spectroscopy, *J. Phys. Chem. B*, 2005, **109**, 24134–24141.
44 H. Jansson and J. Swenson, Dynamics of water in molecular sieves by dielectric spectroscopy, *Eur. Phys. J. E.*, 2003, **12**, 51–54.
45 H. Frauenfelder, G. Chen, J. Berendzen, P. W. Fenimore, H. Jansson, B. H. McMahon, I. R. Stroe, J. Swenson and R. D. Young, A unified model of protein dynamics, *Proc. Natl. Acad. Sci. U. S. A.*, 2009, **106**, 5129–5134.
46 J. Swenson, H. Jansson and R. Bergman, Relaxation processes in supercooled confined water and implications for protein dynamics, *Phys. Rev. Lett.*, 2006, **96**, 247802.
47 N. Agmon, The grotthuss mechanism, *Chem. Phys. Lett.*, 1995, **244**, 456–462.
48 H. Jansson and J. Swenson, The protein glass transition as measured by dielectric spectroscopy and differential scanning calorimetry, *Biochim. Biophys. Acta, Proteins Proteomics*, 2010, **1804**, 20–26.
49 K. Alhgren, C. Olsson, I. Ermilova and J. Swenson, New insights into te protein stabilizing effects of trehalose by comparing with sucrose, *Phys. Chem. Chem. Phys.*, 2023, **25**(32), 21215–21226.
50 C. Angell, Relaxation in liquids, polymers and plastic crystals—strong/fragile patterns and problems, *J. Non-Cryst. Solids*, 1991, **131**, 13–31.
51 C. A. Angell, K. L. Ngai, G. B. McKenna, P. F. McMillan and S. W. Martin, Relaxation in glassforming liquids and amorphous solids, *J. Appl. Phys.*, 2000, **88**, 3113–3157.

 

52 M. Nakanishi and A. P. Sokolov, Protein dynamics in a broad frequency range: Dielectric spectroscopy studies, *J. Non-Cryst. Solids*, 2015, **407**, 478–485.
53 H. Jansson, R. Bergman and J. Swenson, Role of solvent for the dynamics and the glass transition of proteins, *J. Phys. Chem. B*, 2011, **115**, 4099–4109.
54 P. J. Carreau, Rheological equations from molecular network theories, *Trans. Soc. Rheol.*, 1972, **16**, 99–127.
55 J. D. Ferry and H. S. Myers, Viscoelastic properties of polymers, *J. Electrochem. Soc.*, 1961, **108**, 142C–143C.
56 S. Kim, H. V. Sureka, A. B. Kayitmazer, G. Wang, L. W. Swan and B. D. Olsen, Effect of Protein Surface Charge Distribution on Protein– Polyelectrolyte Complexation, *Biomacromolecules*, 2020, **21**, 3026–3037.
57 A. C. Obermeyer, C. E. Mills, X. H. Dong, R. J. Flores and B. D. Olsen, Complex Coacervation of Supercharged Proteins with Polyelectrolytes, *Soft Matter*, 2016, **12**, 3570–3581.
58 R. A. Kapelner and A. C. Obermeyer, Ionic polypeptide tags for protein phase separation, *Chem. Sci.*, 2019, **10**, 2700–2707.